

Thermoresponsive Triblock-Copolymers of Polyethylene Oxide and Polymethacrylates: Linking Chemistry, Nanoscale Morphology, and Rheological Properties

Marcelo Alves da Silva, Peter Haddow, Stewart B. Kirton, William J. McAuley, Lionel Porcar, Cécile A. Dreiss, and Michael T. Cook*

Thermoreversible gels switch from a free-flowing liquid state to an elastic gel mesophase upon warming, displaying the reverse transition upon cooling. While this phenomenon makes these advanced materials highly attractive in numerous fields, the generation of optimal materials of tailored rheology and transition temperatures is stifled by the lack of design principles. To address this need, a library of ABA copolymers has been prepared with “A” blocks exhibiting thermoresponsive behavior and “B” blocks of poly(ethylene glycol). This library evaluates the effect of “A” chemistry, probing three polymer classes, and A/B block molecular weight on thermally-induced phase changes in solutions of the polymers. An exploration by rheometry coupled to Small-Angle Neutron Scattering (SANS) elucidates temperature-dependent hierarchical self-assembly processes occurring on the nanoscale as well as bulk rheology. This process deciphered links between rheology and supracolloidal assemblies (sphere, ellipses, and cylinders) within the gel state with interactions probed further via structure factors. Several design principles are identified to inform the genesis of next-generation thermoreversible gels, alongside novel materials exhibited thermoresponsive behavior in the solution state for use in applied healthcare technologies.


1. Introduction

The induction of phase changes with temperature as a stimulus can enable triggering of material adaptations by mild warming

M. A. da Silva, P. Haddow, S. B. Kirton, W. J. McAuley, M. T. Cook
School of Life and Medical Sciences
University of Hertfordshire
Hatfield, Hertfordshire AL10 9AB, UK
E-mail: m.cook5@herts.ac.uk

L. Porcar
Institut Laue Langevin
71 Avenue des Martyrs, Grenoble 38042, France

C. A. Dreiss
Institute of Pharmaceutical Science
King's College London
Franklin-Wilkins Building, 150 Stamford Street, London SE1 9NH, UK

 The ORCID identification number(s) for the author(s) of this article can be found under <https://doi.org/10.1002/adfm.202109010>.

© 2021 The Authors. Advanced Functional Materials published by Wiley-VCH GmbH. This is an open access article under the terms of the Creative Commons Attribution License, which permits use, distribution and reproduction in any medium, provided the original work is properly cited.

DOI: 10.1002/adfm.202109010

or even touch, where the warmth of the body induces a physical transition.^[1] “Thermoreversible gelators” may be designed such that this warming process induces the reversible sol-gel transition of a polymer solution,^[2] a phase change from a low viscosity solution state to a viscoelastic gel phase above a critical temperature (T_{gel}). These materials are particularly useful in healthcare when T_{gel} occurs between room and body temperature ($\approx 37^\circ\text{C}$) allowing for in situ gel formation. Thermoreversible gelators are attractive in parenteral drug delivery where the material may be injected in the solution state before forming a gel depot which sustains delivery of drugs.^[3] In topical medicines, temperature-induced in situ gelation occurring between room and body temperature enhances retention while allowing easy application.^[4,5] Gel formation after administration is attractive in wound healing where the materials may fill a burn cavity before forming a gel.^[6]

The materials are also being extensively explored for cell culture, tissue engineering and bioprinting applications due to the induction of gel formation under mild conditions which are less hazardous to cells than chemical cross-linkers.^[7–9] The most commonly reported thermoreversible gelator is poloxamer 407 (or Pluronic F127), poly(ethylene oxide)₁₀₀-b-poly(propylene oxide)₆₅-b-poly(ethylene oxide)₁₀₀, however this material has several drawbacks, including low gel strengths for applications under shear,^[10] highly concentration-dependent T_{gel} ,^[4,11] and rapid dissolution in excess fluid.^[12] Thus, there is a need to develop the next-generation of thermoreversible gelators with enhanced functionality.

Polymers exhibiting lower critical solution temperatures (LCSTs) respond to heating by an entropically-driven desolvation, which may be used as a mechanism to design thermoreversible gelators. ABA block copolymers containing A blocks with LCSTs and a hydrophilic B block have been shown to exhibit this behavior. For example, Lin and Cheng demonstrated the thermoreversible gelation of a poly(N-isopropylacrylamide)-b-poly(ethylene glycol)-b-poly(N-isopropylacrylamide) (PNIPAM-b-PEG-b-PNIPAM) block copolymer in aqueous solution, observing the formation of hard gels relative to a PNIPAM-b-PEG copolymer.^[13] This thermoreversible

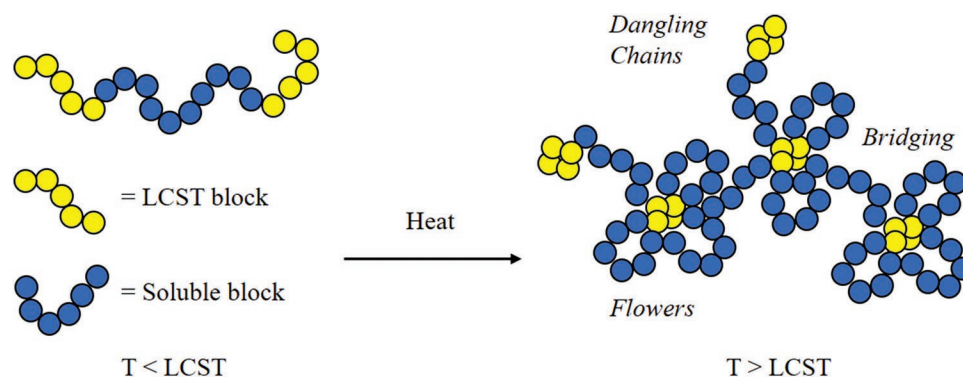


Figure 1. Proposed mechanism of gelation in ABA block copolymers with thermoresponsive “A” blocks with an LCST and solvophilic “B” blocks.

gelation has also been observed in PNIPAM-*b*-poly(*N,N'*-dimethylacrylamide)-*b*-PNIPAM^[2] and PNIPAM-*b*-poly(*N*-vinylpyrrolidone)-*b*-PNIPAM,^[14] for example, and in poly(*N*-vinylcaprolactam)-*b*-PEG-*b*-poly(*N*-vinylcaprolactam)^[15] where poly(*N*-vinylcaprolactam) also exhibits an LCST. ABA block copolymers of this type undergo a transition from entirely solvophilic below the LCST to an amphiphilic state when heated above the LCST, where the A blocks become increasingly solvophobic. It has been theorised that in this state where a solvophilic block (B) is flanked by two relatively solvophobic blocks (A) the polymer may be able to form “flowerlike” micelles, with bridging occurring due to polymer chains being able to associate neighbouring micelles.^[16,17] This theory follows that of Semenov and co-workers,^[18] which postulates that telechelic polymers (solvophilic polymers with small solvophobic end groups) may exist in three states in solution: as loops of a flowerlike micelle, as a bridge between two flowers, or as a chain “dangling” from a flower with one solvophobic group in the micelle core and the other in the micelle corona, illustrated in **Figure 1**. This model has been further demonstrated in Monte-Carlo simulations.^[19] These studies support interpretation of the gelation processes in thermoresponsive ABA copolymers which may be considered pseudo-“telechelic” above the LCST, but the intimate link between nanoscale morphology and bulk rheology is poorly understood, with a lack of experimental data.^[20] Knowledge gained in this area would inform the rational design of future thermoreversible gelators with enhanced functionality.

This study aims to elucidate the nanoscale processes underpinning gelation in thermoreversible gelators based on ABA copolymers. These copolymers are based on a blueprint where the “A” block exhibits an LCST and the “B” block is the hydrophilic polymer PEG. The effect of molecular weight and LCST-exhibiting polymer type is investigated, exploring materials containing PNIPAM, poly(2-*N*-(dimethylamino)ethyl methacrylate) (PDMAMA), and poly(diethylene glycol methyl ether methacrylate) (PDEGMEMA).

2. Results and Discussion

α -Bromoisobutyryl groups were covalently bound to both terminal alcohol groups of 5 and 10 kDa PEG to form ATRP macroinitiators. The chemical structure was unambiguously confirmed by ¹H and DOSY NMR (Figure S1 and S2, Supporting Information). The ratio of integrals of the CH₂

with the PEG chain (3.7 ppm) and the C(CH₃)₂ of the two α -bromoisobutyryl moieties (1.8 ppm) confirmed complete conversion of the terminal alcohol groups to the ATRP initiator functionality. ¹H DOSY NMR demonstrated that hydrogen atoms associated with the PEG backbone and functionalised ends showed the same diffusion coefficients, further supporting their covalent attachment to PEG. A library of ABA copolymers consisting of a thermoresponsive block (A) and PEG (B) were then synthesised by ATRP from the difunctional PEG macroinitiators. This library was composed of 3 classes of triblock copolymer where the A block was either PNIPAM, PDMAMA, or PDEGMEMA (**Figure 2**). The molecular weight of the constituent blocks was controlled so that the copolymers had the following structures: 10 kDa A-*b*-5 kDa B-*b*-10 kDa A, 10 kDa A-*b*-10 kDa B-*b*-10 kDa A, and 20 kDa A-*b*-10 kDa B-*b*-20 kDa A (designated A10-B5-A10, A10-B10-A10 and A20-B10-A20 when discussing architecture class, with specific sample IDs in Figure 2), allowing for understanding of the effect of each block’s molecular weight on polymer properties in solution as thermoreversible gelators.

The successful synthesis of ABA copolymers was confirmed by ¹H NMR and GPC. The ¹H NMR of each triblock copolymer with peak assignment is shown in Figure S2 in the Supporting Information, confirming successful conversion of monomer to polymer. The molecular weights for each block were calculated using ¹H NMR. ¹H NMR confirmed that monomer conversion gave clear discrimination between low and high levels at molecular weights of \approx 10 and 20 kDa (Figure 2). These levels were selected based on the molecular weights shown to exhibit gelation and pilot studies on maximal conversion using ATRP in these polar media required for PEG solubilisation.^[21] GPC gave the PDI of each copolymer and confirmed that molecular weight distributions were monomodal with no residual unreacted PEG (Figure S3, Supporting Information). This was further supported with DOSY NMR (Figure S4, Supporting Information). PDEGMEMA and PDMAMA copolymers had PDIs ranging from 1.09 – 1.32 while the PNIPAM samples had PDIs >1.8. The ATRP of PDMAMA and PDEGMEMA achieved well defined polymers of low polydispersity. This lower level of control in PNIPAM is attributed to the use of water as a solvent which has been shown to adversely affect the deactivation processes controlling ATRP via reversible dissociation of the halide ligand from the Cu(II) ATRP deactivator, amongst other processes.^[22] However, pilot studies indicated that water was required to achieve this conversion while solubilising PEG.

Chemical Structure	Polymer ID	Mn of PEG (kDa) [DP]	Mn of arm (kDa) [DP]	PDI
	N10-P5-N10	5.4 [123]	12.8 [113]	2.6
	N10-P10-N10	10.8 [245]	11.1 [98]	1.88
	N20-P10-N20	10.8 [245]	22.3 [197]	1.84
	D10-P5-D10	5.4 [123]	11.4 [72]	1.24
	D10-P10-D10	10.8 [245]	12.7 [80]	1.14
	D20-P10-D20	10.8 [245]	18.1 [115]	1.32
	DEG10-P5-DEG10	5.4 [123]	10.2 [54]	1.18
	DEG10-P10-DEG10	10.8 [245]	10.3 [55]	1.13
	DEG20-P10-DEG20	10.8 [245]	19.9 [106]	1.09

Figure 2. Structure of NIPAM (blue), DMAEMA (red), and DEGMEMA (green) moieties (left) with polymer ID, molecular weight of constituent blocks (determined by ^1H NMR, with degree of polymerisation (DP)), and PDI as determined by GPC (right).

Initial studies by vial inversion indicated that copolymer solutions in water at a concentration of 20% (w/v) exhibited an increase in viscosity upon warming. This thickening was investigated by small-amplitude oscillatory shear rheology as a function of temperature (Figure 3). All samples demonstrated an increase in G' or G'' with temperature, reflecting an overall increase in viscoelasticity. Gelation is typically considered to be achieved when $G' > G''$,^[23] indicating a dominance of elastic behavior over dissipative viscous flow, which occurs at the critical gelation temperature. PNIPAM and PDEGMEMA A10-B5-A10 systems exhibited a stepwise transition to a more viscous state, without achieving the formation of a “rheological” gel, with G'' dominant at all temperatures. PDMAEMA with the same A10-B5-A10 architecture was highly viscoelastic and predominantly solid-like at all temperatures, with minor thickening occurring during heating to 50 °C. PDMAEMA copolymers with A10-B10-A10 and A20-B10-A20 architectures also exhibited this phenomenon, where dissipated energy dominating the rheogram, albeit with lower values of the moduli. Architectures with a larger PEG block, A10-B10-A10 and A20-B10-A20, exhibited a T_{gel} with PNIPAM and PDEGMEMA blocks, transitioning to a state with $G' > G''$, with the transition with PNIPAM being sharper and leading to a plateau in G' , compared to PDEGMEMA. Based on these results, it was hypothesised that 1) the morphologies formed by the 5 kDa PEG constructs is distinct from the materials with a 10 kDa PEG block, since they do not lead to gelation and 2) PDMAEMA-based materials have a morphology different from PNIPAM and PDEGMEMA, since they remained predominantly viscous solutions. Frequency sweeps of the 20% (w/v) solutions was also conducted at 25 and 50 °C (Figure S6) and the effect of architecture was explored by comparison of DEGMEMA copolymers. All solutions were predominantly liquid-like at 25 °C with great frequency dependence. At

50 °C, above T_{gel} , the DEG10-P5-DEG10 copolymer exhibited a frequency dependence with $G'' > G'$ over the temperatures measured, in a manner indicative of a viscoelastic liquid. DEG10-P10-DEG10 and DEG20-P10-DEG20 were gels exhibiting $G' > G''$ at all frequencies. To assess the effect of LCST component, frequency sweeps of D10-P10-D10 and N10-P10-N10 were also conducted at 50 °C (Figure S7). In-line with temperature ramps, D10-P10-D10 remained a viscous liquid ($G'' > G'$) at all frequencies, while N10-P10-N10 exhibited $G' > G''$ across the frequency range, indicative of a gel state.

Dynamic light scattering measurements were conducted to measure the size of the aggregates. Dilute solutions (1 mg/mL) of PNIPAM and PDEGMEMA materials exhibited sharp increases in scattering intensity above a critical temperature (Figure S8), associated with the formation of nanostructures of PDI < 0.2. The hydrodynamic diameter (D_{H}) and ζ -potential were measured at a fixed temperature of 50 °C to initially characterise the nanoparticles (Table S2, Supporting Information). Generally, A10-B5-A10 copolymers formed nanoparticles of larger D_{H} than A10-B10-A10 systems (at 50 °C), indicating the importance of PEG molecular weight on the structure of the nanoparticles, with shorter PEG chains appearing to lead to larger nanoparticles. Additionally, the A20-B10-A20 copolymers formed particles of larger D_{H} than the A10-B10-A10 constructs when using PNIPAM or PDMAEMA as the thermoresponsive component, but no effect was seen in the PDEGMEMA materials. SANS was then employed in an attempt to establish more meaningful relationships between self-assembled polymer morphology and bulk rheology of the gel.^[24]

For each ABA polymer, four temperatures were investigated to capture the behavior across the gelation process, namely: 25, 37, 40 and 50 °C, where 25 °C lies well below the LCST, 37 and 40 °C around the expected onset of the transition and 50 °C

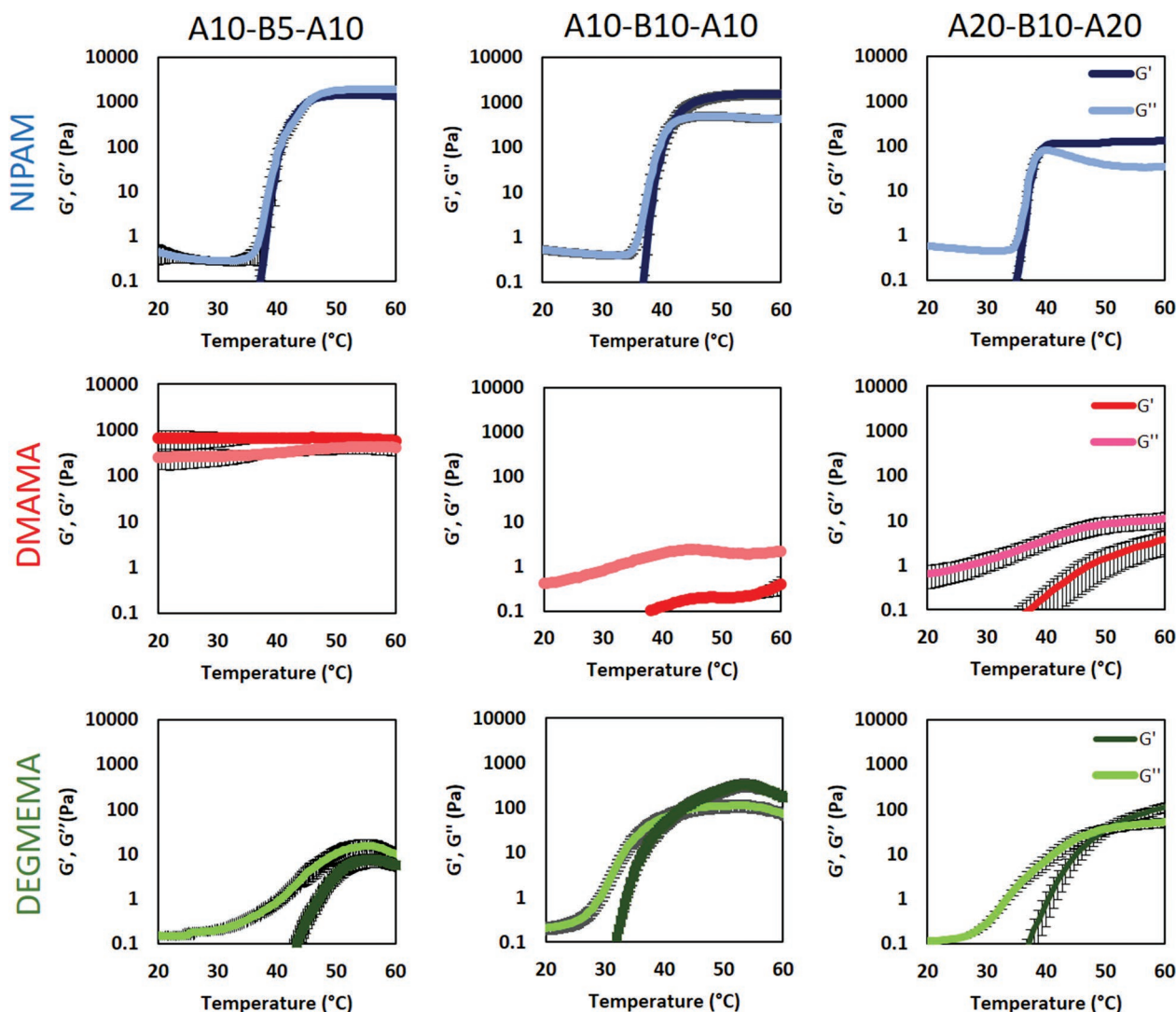


Figure 3. Rheograms showing the effect of temperature on G' (dark) and G'' (light) of PNIPAM (blue), PDMAMA (red), and PDEGMEMA (green) ABA copolymer solutions at 20% (w/v). Temperature ramps conducted at an oscillatory shear stress within the linear viscoelastic region of the sample at 25 °C (1 Pa) and a frequency of 1 Hz.

well above the transition. Two concentrations, 5 and 20% (w/v), were explored for each temperature. In dilute 5% (w/v) systems, the SANS data were fitted using only a form factor $P(q)$, where possible, while in concentrated 20% (w/v) systems, interactions between the scattering centres are significant, and a structure factor $S(q)$ was also required. Structural information can be extracted from $P(q)$, while $S(q)$ provides insights on the nature of the interaction between the scattering centres.^[25] The manuscript describes the major findings from the SANS study with specific values from the fitted parameters provided in the Supporting Information (Tables S3–S11, Supporting Information).

PNIPAM is a model thermoresponsive polymer, and a wealth of information about its behavior is available in the literature.^[20] The behavior of PNIPAM-*b*-PEG-*b*-PNIPAM is initially probed as a reference for comparison to the other two ABA polymer classes (Figure 4).

PNIPAM-*b*-PEG-*b*-PNIPAM constructs showed two distinct behaviors dependent on the molecular weight of the

constituting blocks as a function of the temperature. At 25 °C, the SANS patterns are best fitted with the polymeric Gaussian coil model (PGC),^[26] a model that describes the behavior of polymer chains in a *theta* solvent. In this case, the SANS signal does not come from micellar aggregates, but from a concentration distribution of solvated polymer coils. The radius of gyration is not sensitive to the polymer architecture. N10-P5-N10, N10-P10-N10 and N20-P10-N20 have radii of gyration of ≈ 35 – 40 Å at 5% (w/v), suggesting that the coils are not fully extended objects but collapsed coils (Tables S3 and S5, Supporting Information).

At 37 °C and above, the SANS data were fitted using two form factors, a polymeric Gaussian chains model ($P(q)$ PGC), combined with a core-shell sphere form factor ($P(q)$ CS sphere). This shows, above the LCST, a major change in the morphology of scattering objects, namely, the presence of micelles. The micellar aggregates have sufficient internal contrast that SANS can resolve its core from the shell. In

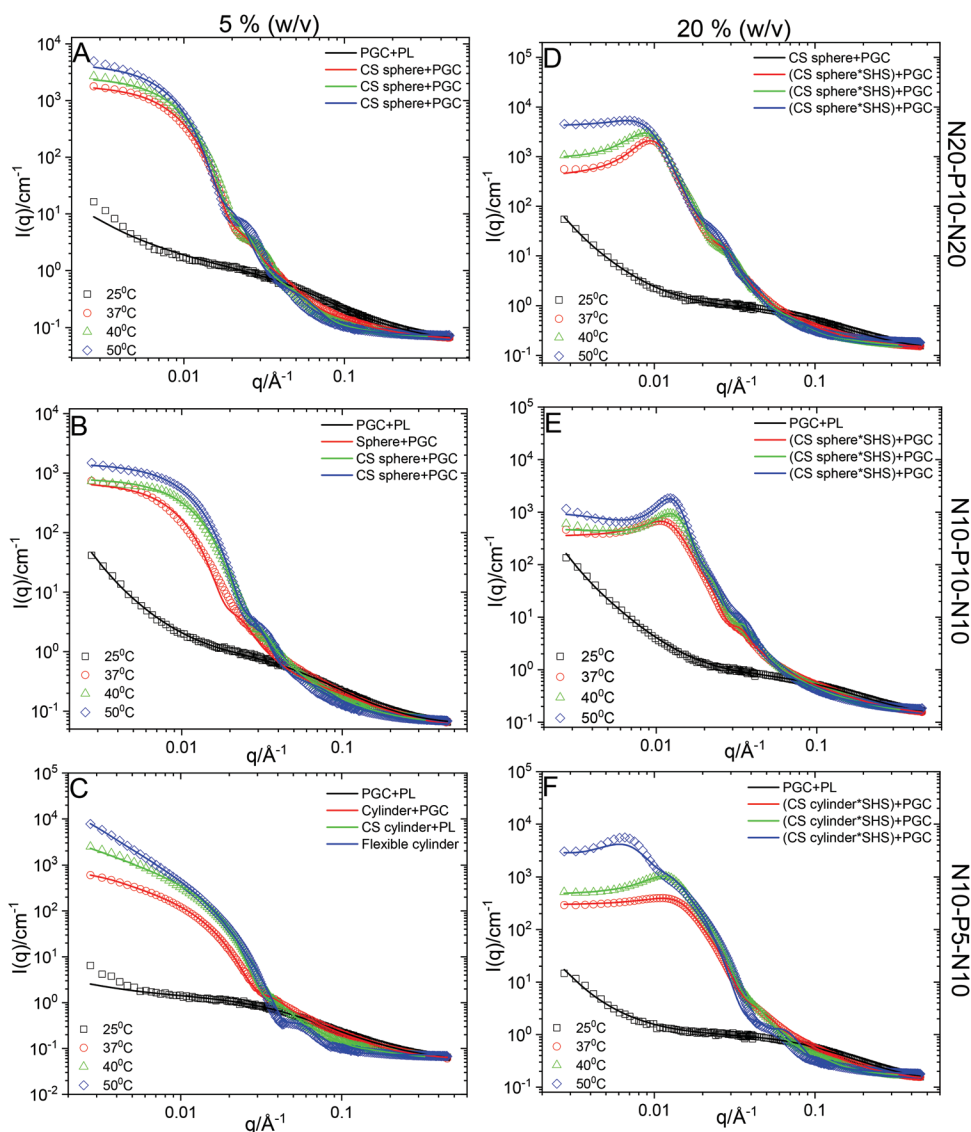


Figure 4. SANS data (open symbols) and fits (solid lines) for PNIPAM-*b*-PEG-*b*-PNIPAM (NX- PY-NX) copolymers as a function of concentration, temperature and copolymer ratios. CS, core-shell; PGC, polymeric Gaussian coil; PL, power law; SHS, sticky hard-sphere, respectively. Concentration is shown above graphs, with architecture on the right.

this case, the core is significantly drier than the shell. For instance, for 5% (w/v) N10-P10-N10 at 40 °C, the core scattering length density (SLD) is $\approx 1.6 \cdot (10^{-6} \cdot \text{\AA}^{-2})$ while the shell SLD is $\approx 6.0 \cdot (10^{-6} \cdot \text{\AA}^{-2})$ (Table S4, Supporting Information). This approximates to a shell with 94% D₂O and a core containing 15% D₂O, calculated against a hypothetical dry core constituted entirely of PNIPAM (SLD = $0.707 \cdot (10^{-6} \cdot \text{\AA}^{-2})$), based on repeat unit C₈H₁₅O₂N, ($\rho = 1.023 \text{ g} \cdot \text{cm}^{-3}$) and a shell containing only PEG (SLD = $0.679 \cdot (10^{-6} \cdot \text{\AA}^{-2})$), based on repeat unit C₂H₄O, ($\rho = 1.2 \text{ g} \cdot \text{cm}^{-3}$). This suggests a core mostly formed by PNIPAM blocks, while the shell is highly hydrated, likely formed mostly by PEG chains. The presence of D₂O in the core is consistent with PNIPAM retaining some level of solvation, even above the LCST.^[27] For N10-P10-N10 5% (w/v) at 37 °C (Figure 4B), the SANS data were better described as spheres, rather than core-shell spheres, suggesting a lack of segregation of PNIPAM and PEG blocks. Above 37 °C, a core-shell sphere model is required

to better describe the SANS data, suggesting that segregation may take place as the temperature increases, consistent with the transition occurring across this range observed with rheology (Figure 3) and prior studies of the phase separation of PNIPAM.^[28] A larger core and shell are observed with an increase in PNIPAM size (N20-P10-N20). For instance, the shell and core radius of N10-P10-N10 5% (w/v) are 75 and 168 Å at 40 °C (Table S3, Supporting Information). It is also notable that the contribution of the polymeric Gaussian coil form factor (P(q)PGC) signal diminishes as the temperature increases from 37 to 50 °C, as measured by changes of the fitting parameters A and B. P(q)PGC can arise from free polymer coils that gradually become incorporated into the micellar aggregates as temperature increases, but could also arise from the chains in the micelle corona, and its reduced contribution thus corresponding to a reduction in “dangling chains” of the ABA copolymer or restricted motion of PEG chains occurring with desolvation.

In contrast to the other two constructs, SANS data for the N10-P5-N10 polymer could not be fitted using spherical objects (Table S5, Supporting Information). As the temperature changed from 37 to 40 and 50 °C, best fits were obtained with a cylinder, then a core-shell cylinder and then a flexible cylinder form factor, at these respective temperatures, showing some evolution with the temperature. The elongated shapes obtained are consistent with the shorter PEG blocks, which cannot accommodate the curvature required for spherical micelles, which is reflected in the larger DH measured by dynamic light scattering previously.

At 20% (w/v), a structure factor is required to account for interparticle interactions. For all three PNIPAM-PEG-PNIPAM constructs, the structure factor that best fitted the data was the sticky hard-sphere (SHS).^[29–31] The hard-sphere model (HS)^[31,32] describes a repulsive short-range interaction arising from excluded volume interactions. The sticky hard-sphere model adds a middle range attractive element to the hard-sphere model, described as “stickiness”, which takes a lower value for systems with greater attraction.^[29] The main contribution of this model is to show that the micellar aggregates have an interparticle attractive interaction that increases with temperature. For instance, the stickiness values for N10-P10-N10 20% (w/v) at 37, 40, and 50 °C are 0.468, 0.241, and 0.122, respectively (Table S4, Supporting Information). A similar trend is observed for N20-P10-N20 (0.887, 0.465, and 0.463, respectively, Table S3, Supporting Information). For the construct with the smaller PEG block (N10-P5-N10) (Figure 4C,F), the scattering curves differ markedly from the two other constructs; it was difficult to achieve a satisfactory fit, but, overall, the data could be fitted with a core-shell cylinder and a sticky-hard-sphere structure factor. While the sticky-hard-sphere structure factor cannot strictly be applied to cylinders, it does at least reflect the absence of attractive interactions between micelles for this construct, with values always greater than 1. Taken together, the elongated shape of the aggregates (seen at 5%) and the reduced stickiness for N10-P5-N10 depart from the behavior of the other two constructs, and is in line with the weaker rheological response with $G'' < G'$ at all temperatures probed (Figure 3).

The PDMAMA-b-PEG-PDMAMA (Dx-Py-Dx) polymer set shows a remarkably similar (Figure 5), yet subtly different behavior than PNIPAM-PEG-PNIPAM (Figure 4). PDMAMA-b-PEG-b-PDMAMA also produces spherical micellar aggregates above the LCST of PDMAMA, however, the micellar aggregates do not show the segregation observed for PNIPAM-b-PEG-PNIPAM and are better described as spheres rather than core-shell spheres. Generally, micellar aggregates generate core-shell structures as the hydrophilic blocks are hydrated while the hydrophobic core is dry. While the SLD of the constituents of the shell and core might be similar, a wet shell and a dry core create a SLD difference large enough to be observable by SANS. For PDMAMA-b-PEG-b-PDMAMA, this differentiation is not observed, suggesting either a relatively wet core (leading to similar SLDs) or a weaker segregation between the blocks. The SLD for the whole aggregate fluctuates around 5.7 for D10-P10-D10 (Table S10, Supporting Information), which is equivalent to the SLD of a mixture of 89% D₂O/11% PDMAMA-b-PEG-b-PDMAMA. PDMAMA-b-PEG-b-PDMAMA data above the LCST were also fitted by a combination of two

form factors: spheres and polymeric Gaussian coils, with the contribution from P(q)PGC diminishing as the temperature increases, as observed with the PNIPAM-based construct.

At 5% (w/v), a weak interparticle interaction contribution is necessary to fit the data, unlike for PNIPAM-PEG-PNIPAM. Therefore, data sets at both 5 and 20 wt% were fitted with a structure factor. The “stickiness” is higher than for PNIPAM-PEG-PNIPAM and shows very limited temperature dependence up to 50 °C for D10-P10-D10 20% (w/v): the stickiness at 37, 40, and 50 °C is 1.2, 1.8 and 0.52, respectively and a weak temperature dependence in all cases for D20-P10-D20: 0.64, 0.54 and 0.74, respectively (Tables S11, S10). This suggests, overall, a weaker attraction in the system than PNIPAM-b-PEG-b-PNIPAM.

Another major difference from PNIPAM-b-PEG-b-PNIPAM systems is the behavior below the LCST. At 25 °C, PDMAMA-b-PEG-b-PDMAMA data are better fitted using spheres for D20-P10-D20 (Figure 5A,D), ellipsoids for D10-P10-D10 (Figure 5B,E) and cylinders for D10-P5-D10 (Figure 5C). This suggests that PDMAMA-PEG-PDMAMA copolymers are already forming aggregates even below the transition observed by rheology. This could be attributed to the molecular weight dependence of the LCST transition seen in PDMAMA, resulting in the higher molecular weight chains transitioning to a micellar form at temperatures below 25 °C.^[33]

As seen for the PNIPAM construct, the morphology of the polymer with the shorter PEG block (D10-P5-D10) deviates strongly from both D20-P10-D20 and D10-P10-D10, forming elongated cylindrical aggregates above the LCST. In contrast with the PNIPAM-b-PEG-b-PNIPAM polymers (Table S5, Supporting Information), D10-P5-D10 (Table S11, Supporting Information) data suggest shorter and less flexible cylinders. At 5 wt%, N10-P5-N10 cylindrical aggregates are always longer than 1000 Å above the LCST, while the size of D10-P5-D10 aggregates start at 700 Å around LCST and only reaches values of ≈1000 Å at 50 °C which supports the macroscopic behavior observed, as D10-P5-D10 20% (w/v) solutions are exceedingly viscous and were not investigated by SANS due to difficulty in manipulating the samples (Table S11, Supporting Information). It is inferred from the dilute regime that the presence of cylinders of indeterminate (>1000 Å) length even below the LCST (Figure 5) can lead to network formation and thus a gel state across the entire rheogram (see the Supporting Information for expanded discussion).

PDEGMEMA-b-PEG-b-PDEGMEMA copolymers follow similar trends as the two constructs previously described (Figure 6). Above the LCST, micellar aggregates are observed. The SANS data above the LCST require two contributions: one for the aggregates and another for the polymer chains. Unlike the other two systems, each PDEGMEMA-b-PEG-b-PDEGMEMA architecture studied required a different form factor for the micellar aggregates: DEG20-P10-DEG20 (Figure 6A,D) is better described by core-shell spheres, DEG10-P10-DEG10 (Figure 6B,E) by ellipsoids and DEG10-P5-DEG10 (Figure 6C,F), similar to the other two copolymers (Figure 4C,F and 5C), is better described by cylindrical objects. In contrast, with PNIPAM-b-PEG-b-PNIPAM, core-shell spheres were observed for both N10-P10-N10 (Figure 4B,E) and N20-P10-N20 (Figure 4A,D) constructs, and with PDMAMA-b-PEG-b-PDMAMA, spheres were

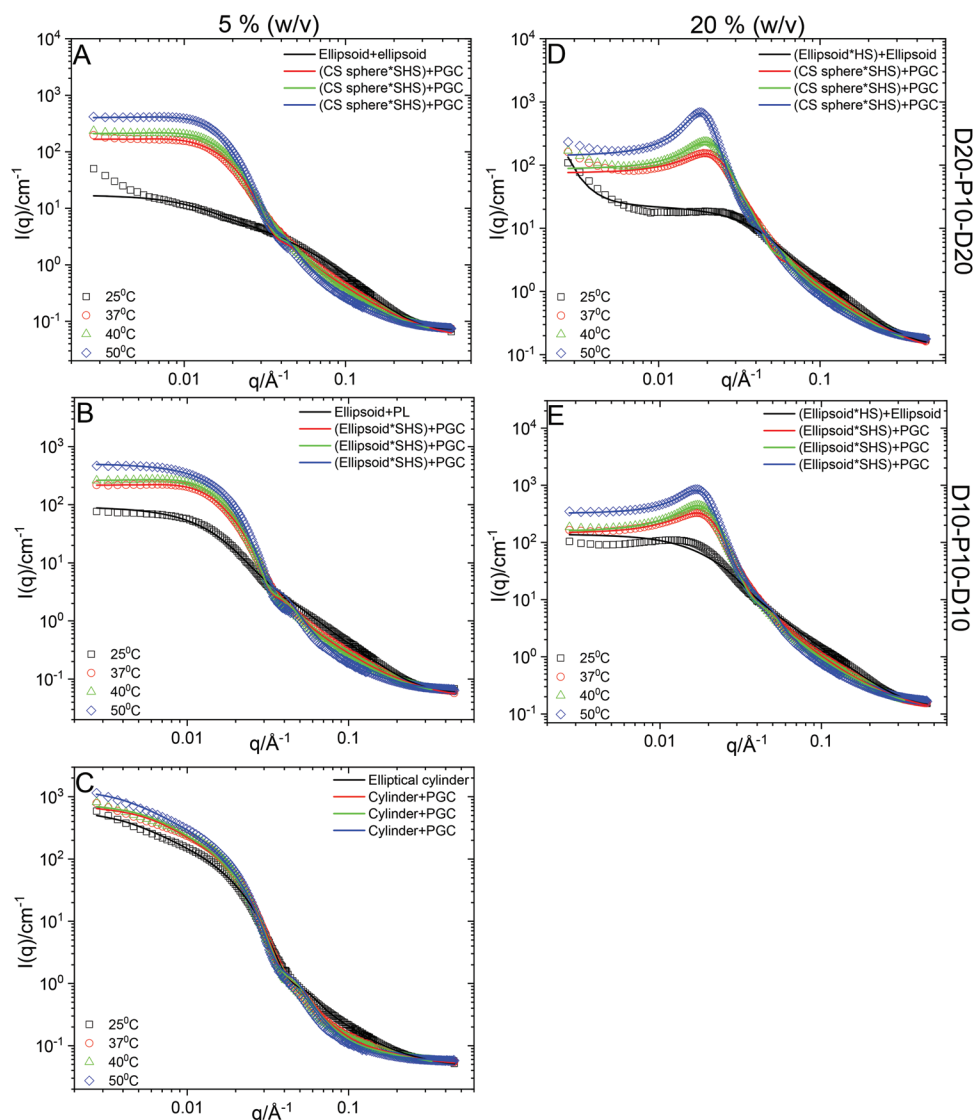


Figure 5. SANS data (open symbols) and fits (solid lines) for PDMAMA-b-PEG-b-PDMAMA (Dx-Py-Dx) copolymers as a function of concentration and temperature and copolymer ratios. Concentration is shown above graphs, with architecture on the right.

observed. Notably, for all three P5 architectures (short PEG block architecture), cylinders were obtained independently of the polymer chemistry (Figure 4–6C).

For DEG10-P10-DEG10, the data could be fitted both as plain ellipsoids or highly polydisperse spheres, in either case, the data could not be fitted adequately with a core-shell structure. Similar to PDMAMA-b-PEG-b-PDMAMA (Figure 5B,E), this lack of segregation between the blocks suggests a relatively wet core. However, the whole aggregate is drier than the PDMAMA-b-PEG-b-PDMAMA aggregates. At 20% (w/v), the SLD for the DEG10-P10-DEG10 is ≈ 3.5 ($10^{-6} \cdot \text{\AA}^{-2}$) (Table S7, Supporting Information), which is equivalent to a 50% mixture $\text{D}_2\text{O}/\text{DEG10-P10-DEG10}$, while for D10-P10-D10, the aggregate SLD is estimated to be ≈ 5.7 ($10^{-6} \cdot \text{\AA}^{-2}$) (Table S10, Supporting Information) equivalent to a 89% mixture $\text{D}_2\text{O}/\text{DEG10-P10-DEG10}$. With the larger PEG block, DEG20-P10-DEG20, a core-shell structure is required to fit the data. This particular

case highlights both the impact of 1) the chemical nature of the polymer, as PNIPAM induces more segregation between core and shell, for all architectures (Figure 4), while PDEGMEMA and PDMAMA core and shell are largely indistinguishable (Figures 5 and 6), and 2) the polymer architecture, where the balance between the length of PDMAMA/PEG blocks affects the level of segregation between the core and shell.

PDEGMEMA-b-PEG-b-PDEGMEMA data at 5 and 20% (w/v) required a structure factor to account for interparticle interactions. The architecture plays a strong role in the strength of the attractive interaction. For DEG10-P10-DEG10 (Table S7, Supporting Information), the stickiness is larger than for PNIPAM-b-PEG-b-PNIPAM (Table S4, Supporting Information), 1.23, 1.83, 0.68 for DEG10-P10-DEG10 20wt% at 37, 40 and 50 °C, respectively versus 872, 0.24, 0.12, for N10-P10-N10 20 wt% at 37, 40 and 50 °C, respectively, and only drops strongly at 50 °C, while for DEG20-P10-DEG20, the

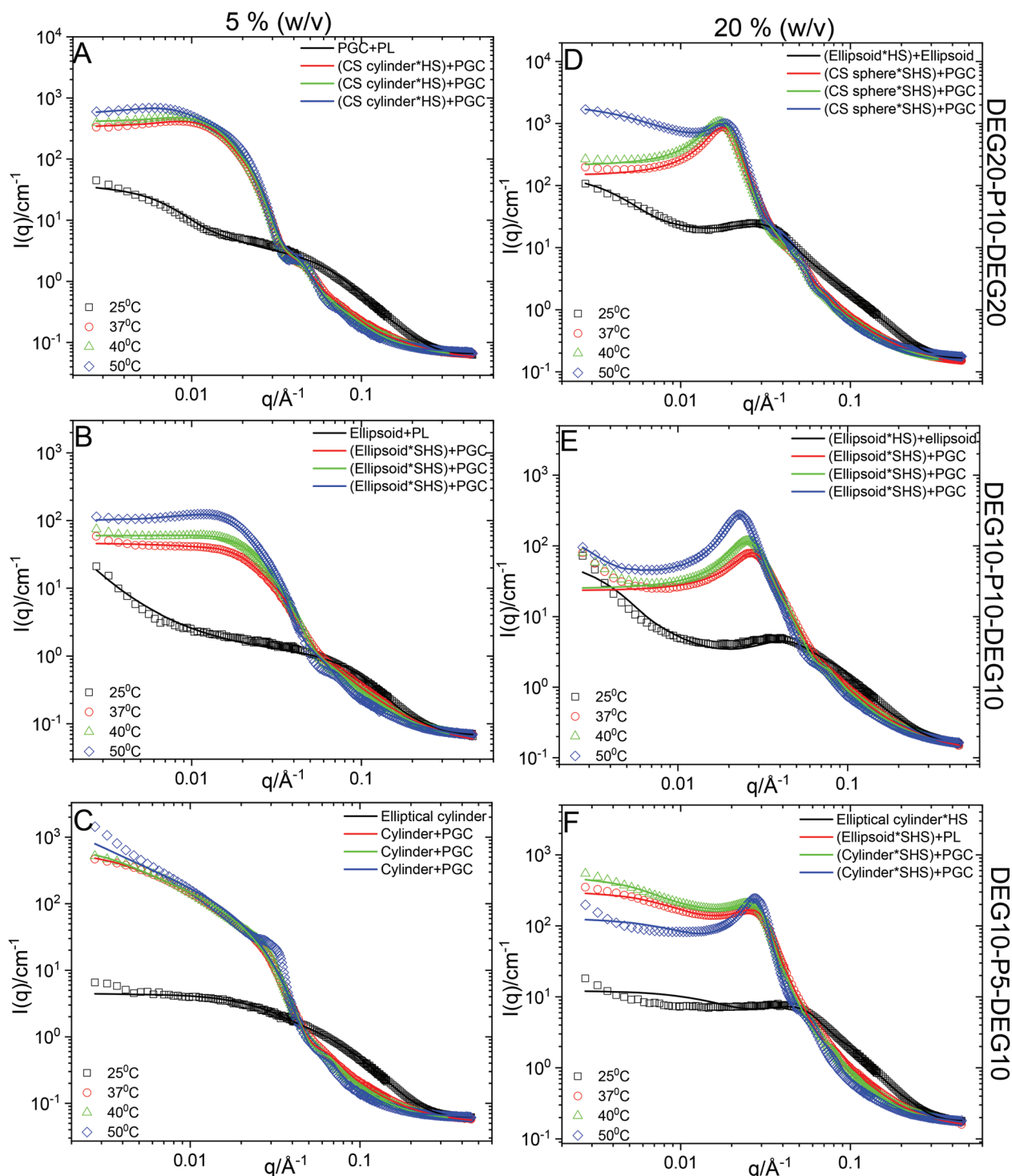


Figure 6. SANS data (open symbols) and fits (solid lines) for PDEGMEMA-*b*-PEG-*b*-PDEGMEMA (DEG_x-Py-DEG_x) copolymers as a function of concentration and temperature and copolymer. Concentration is shown above graphs, with architecture on the right.

stickiness is strongly temperature-dependent, changing from 1.65, to 0.887 and 0.136 at 37, 40, and 50 °C, respectively, highlighting the larger influence the LCST/non-LCST ratio has on PDEGMEMA-*b*-PEG-*b*-PDEGMEMA (Tables S6 and S7, Supporting Information).

Also, similarly to PDMAMA-*b*-PEG-*b*-PDMAMA, SANS data for PDEGMEMA-*b*-PEG-*b*-PDEGMEMA below the LCST (25 °C) were better fitted using well-defined objects instead of Gaussian coils (used for PNIPAM-*b*-PEG-*b*-PNIPAM copolymers). Curiously, DEG20-P10-DEG20 SANS data at 20 °C show

the presence of two objects and were fitted adequately using two ellipsoids form factors, one ellipsoid with a major radius of ≈ 377 Å and another with a major radius of ≈ 375 Å, suggesting strong aggregation even at low temperatures (Table S6, Supporting Information).

DEG10-P5-DEG10 follows the same pattern as N10-P5-N10 and D10-P5-D10: the copolymer forms cylindrical aggregates above the LCST and requires a structure factor at 20% (w/v). This suggests that the cylindrical shape is determined by geometrical constraints largely independent of the chemical nature of the LCST copolymers, as all the three ABA polymers assemble into either spherical or ellipsoidal objects at A10-B10-A10 and A20-B10-A20 architectures, but always into cylindrical objects at A10B5A10 architectures (Table S8, Supporting Information).

Taking the SANS and rheology of the thermoreversible gels together, the following conclusions may be drawn:

- Thermoreversible thickening and gelation is related to the formation of micelles which interact via chemical and physical interactions to form a polymer network resistant to shear.
- Micelles are present in the dilute systems (5% (w/v)), which may be described by a combination of two form factors describing the particle shape and Gaussian coil from the polymer components
- In the concentrated regime (20% (w/v)), a sol-gel transition occurs above a specific temperature. No sol-gel transition was obtained for 1) the PDMAMA-based copolymers (except the A10-B5-A10 architecture), and 2) the A10-B5-A10 architectures (except the PDMAMA-based one). The copolymers with a 5 kDa PEG block formed elongated cylindrical micelles for all three polymer chemistries (Figure 7). “Sticky hard-sphere” structure factors were fitted to all concentrated samples, which is believed to be a result of polymer bridges between nanoparticles which then contribute to overall elasticity of the system.
- Copolymers with a 10 kDa PEG block typically formed spherical micelles interacting via a “sticky hard-sphere” structure factor at high concentrations, which suggests a flower-like micellar morphology bridged by unimer chains (Figure 7). These systems formed gels with predominantly elastic behavior ($G' > G''$) in NIPAM and DEGMEMA copolymers.

- The A20-B10-A20 constructs at 50 °C can all be fitted as spheres/core-shell spheres with sticky sphere structure factors and a contribution from polymer coils in solution, and thus offer the best point of comparison between copolymers. In this case, the D20-P10-D20 copolymers were the least “sticky” of the series, and this relatively low adhesion between particles may contribute to the low elasticity of the gels formed.

The cytotoxicity of the materials was also evaluated against human keratinocytes (HaCat) to highlight the materials with the lowest risk for translation into healthcare (Figure S9). LDH and MTS assays confirmed that PNIPAM and PDEGMEMA-containing triblock copolymers did not destroy the cell membrane or induce a reduction in metabolic activity, respectively. PNIPAM has been observed to exhibit cytotoxicity,^[34] however the majority of publications do not report this.^[20] PDMAMA copolymers all gave a significant indication of cytotoxicity in both assays. PDMAMA has been reported to induce cytotoxicity due to the formation of complexes between the tertiary amine of the monomer unit and the negatively charged proteins bound to the cell membrane, which is expected to disrupt cellular pathways and result in cell death.^[35]

3. Conclusions

ABA triblock copolymers consisting of LCST-exhibiting PNIPAM, PDEGMEMA, or PDMAMA “A” blocks and PEG “B” blocks exhibit a temperature-induced increase in viscosity in aqueous solution. SANS measurements indicate that the nanostructures present in solution depend both on the chemistry of the LCST polymer and the molecular weight of the constituent blocks. The chemistry of the “A” blocks affects both degrees of hydration of this component above the LCST and potential for interaction between nanoparticles. Copolymers with 5 kDa PEG and 10 kDa LCST-exhibiting blocks formed elongated cylindrical structures, and, for NIPAM and DEGMEMA copolymers, displayed a rheogram where the energy from deformation was predominantly

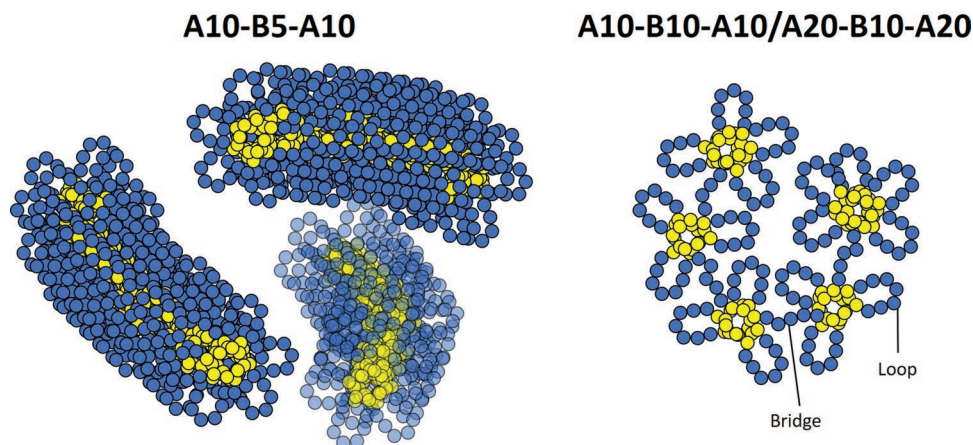


Figure 7. Suggested structures of thermoresponsive polymers in solution at 50 °C, which leads to viscoelastic behavior.

dissipated and was therefore a viscous liquid rather than a gel. In the DMAMA copolymers, this construct was a gel at all temperatures which may in part be related to the formation of cylindrical nanostructures even at the lowest temperatures measured. Copolymers with 10 kDa PEG and 10 or 20 kDa LCST-exhibiting blocks formed spherical or ellipsoidal micellar structures and for NIPAM and DEGEMA copolymers displayed thermoreversible gelation, transitioning to a predominantly elastic state ($G' > G''$). The SANS analysis showed that these spherical and ellipsoidal micelles interacted through “sticky” hard-sphere structure factors, which can be interpreted as the formation of flower-like micelles bridged by unimer chains, a mechanism of gelation found in telechelic polymers. N10-P10-N10 and N20-P10-N20 copolymers formed spherical core-shell micelles with relatively high levels of stickiness and likewise formed superior gels with sharp transition, high values of G' and a long plateau in the gel state. In contrast, DMAMA copolymers with 10 kDa PEG did not form gels and remained predominantly viscous ($G'' > G'$) and exhibited weaker “stickiness” at high temperatures compared to NIPAM copolymers, plausibly indicating a reduction of these stabilising bridges.

These findings have implications for the design of novel thermoreversible gelators, where tuning the morphology of the micellar aggregates (spheres versus ellipsoids versus cylinders) and bridging between them could lead to optimising the temperature response and the elastic character.

4. Experimental Section

Experimental details are contained in the Supporting Information.

Supporting Information

Supporting Information is available from the Wiley Online Library or from the author.

Acknowledgements

M.T.C. and C.A.D. would like to thank the EPSRC EP/T00813X/1 for funding the research position of MAS. M.C., W.J.M., and S.B.K. would also like to thank the University of Hertfordshire for funding PH's PhD studentship. The SANS experiments were performed on beamline D22 at the Institut Laue Langevin (ILL), Grenoble, France (Experiment 9-11-1941: Nanostructure of a library of thermogelling materials based on ABA block copolymers. <https://doi.org/10.5291/ILL-DATA.9-11-1941>). The authors are grateful to Dr. Olga Matsarskaia at the ILL for providing assistance in using beamline D22. P.H. is grateful to Dr. Ewelina Hoffman at the University of Hertfordshire for providing training in cell culture.

Conflict of Interest

The authors declare no conflict of interest.

Data Availability Statement

Research data are not shared.

Keywords

in situ gels, lower critical solution temperatures, temperature-responsive polymers, thermoreversible gels

Received: September 6, 2021

Revised: October 15, 2021

Published online:

- [1] M. A. Ward, T. K. Georgiou, *Polymers* **2011**, *3*, 1215.
- [2] S. E. Kirkland, R. M. Hensarling, S. D. McConaughy, Y. Guo, W. L. Jarrett, C. L. McCormick, *Biomacromolecules* **2008**, *9*, 481.
- [3] A. J. De Graaf, I. I. Azevedo Próspero Dos Santos, E. H. E. Pieters, D. T. S. Rijkers, C. F. Van Nostrum, T. Vermonden, R. J. Kok, W. E. Hennink, E. Mastrobattista, *J. Controlled Release* **2012**, *162*, 582.
- [4] P. Haddow, W. J. McAuley, S. B. Kirton, M. T. Cook, *Mater. Adv.* **2020**, *1*, 371.
- [5] J. Yun Chang, Y. K. Oh, H. Soo Kong, E. Jung Kim, D. Deuk Jang, K. Taek Nam, C. K. Kim, *J. Controlled Release* **2002**, *82*, 39.
- [6] I. R. Schmolka, *J. Biomed. Mater. Res.* **1972**, *6*, 571.
- [7] S. F. Khattak, S. R. Bhatia, S. C. Roberts, *Tissue Eng.* **2005**, *11*, 974.
- [8] S. Dutta, D. Cohn, *J. Mater. Chem. B* **2017**, *5*, 9514.
- [9] M. Taylor, P. Tomlins, T. Sahota, *Gels* **2017**, *3*, 4.
- [10] C. He, S. W. Kim, D. S. Lee, *J. Controlled Release* **2008**, *127*, 189.
- [11] K. Edsman, J. Carlfors, R. Petersson, *Eur. J. Pharm. Sci.* **1998**, *6*, 105.
- [12] G. Niu, F. Du, L. Song, H. Zhang, J. Yang, H. Cao, Y. Zheng, Z. Yang, G. Wang, H. Yang, S. Zhu, *J. Controlled Release* **2009**, *138*, 49.
- [13] H. H. Lin, Y. L. Cheng, *Macromolecules* **2001**, *34*, 3710.
- [14] H. Cong, J. Li, L. Li, S. Zheng, *Eur. Polym. J.* **2014**, *61*, 23.
- [15] I. Negru, M. Teodorescu, P. O. Stanescu, C. Draghici, A. Lungu, A. Sarbu, *Mater. Plast.* **2010**, *35*.
- [16] E. B. Zhulina, O. V. Borisov, *Macromolecules* **2012**, *45*, 4429.
- [17] A. J. De Graaf, K. W. M. Boere, J. Kemmink, R. G. Fokkink, C. F. Van Nostrum, D. T. S. Rijkers, J. Van Der Gucht, H. Wienk, M. Baldus, E. Mastrobattista, T. Vermonden, W. E. Hennink, *Langmuir* **2011**, *27*, 9843.
- [18] A. N. Semenov, J. F. Joanny, A. R. Khokhlov, *Macromolecules* **1995**, *28*, 1066.
- [19] M. Nguyen-Misra, W. L. Mattice, *Macromolecules* **1995**, *28*, 1444.
- [20] M. T. Cook, P. Haddow, S. B. Kirton, W. J. McAuley, *Adv. Funct. Mater.* **2020**, *31*, 2008123.
- [21] M. Teodorescu, I. Negru, P. O. Stanescu, C. Drăghici, A. Lungu, A. Sârbu, *React. Funct. Polym.* **2010**, *70*, 790.
- [22] N. V. Tsarevsky, T. Pintauer, K. Matyjaszewski, *Macromolecules* **2004**, *37*, 9768.
- [23] M. A. Ward, T. K. Georgiou, *Polym. Chem.* **2013**, *4*, 1893.
- [24] C. Dreiss, M. T. Cook, L. Porcar, Y. Gerelli, P. Haddow, J. Omar, *Nanostructure of a Library of Thermogelling Materials based on ABA Block Copolymers* **2020**, <https://doi.org/10.5291/ILL-DATA.9-11-1941>.
- [25] D. Qiu, C. A. Dreiss, T. Cosgrove, A. M. Howe, *Langmuir* **2005**, *21*, 9964.
- [26] O. Glatter, O. Kratky, *Small Angle X-Ray Scattering*, Academic Press, Cambridge, MA **1982**.
- [27] R. Pelton, *J. Colloid Interface Sci.* **2010**, *348*, 673.
- [28] M. T. Cook, S. K. Filippov, V. V. Khutoryanskiy, *Colloid Polym. Sci.* **2017**, *295*, 1351.
- [29] S. V. G. Menon, C. Manohar, K. S. Rao, *J. Chem. Phys.* **1991**, *95*, 9186.
- [30] R. J. Baxter, *J. Chem. Phys.* **1968**, *49*, 2770.
- [31] M. Kotlarchyk, S. H. Chen, *J. Chem. Phys.* **1983**, *79*, 2461.
- [32] J. K. Percus, G. J. Yevick, *Phys. Rev.* **1958**, *110*, 1.
- [33] V. Bütün, S. P. Armes, N. C. Billingham, *Polymer* **2001**, *42*, 5993.
- [34] H. Vihola, A. Laukkanen, L. Valtola, H. Tenhu, J. Hirvonen, *Biomaterials* **2005**, *26*, 3055.
- [35] J. Cai, Y. Yue, D. Rui, Y. Zhang, S. Liu, C. Wu, *Macromolecules* **2011**, *44*, 2050.